

This is an Open Access document downloaded from ORCA, Cardiff University's institutional repository: <https://orca.cardiff.ac.uk/id/eprint/109338/>

This is the author's version of a work that was submitted to / accepted for publication.

Citation for final published version:

Liang, Xiaoyu, Li, Xuanling, Duan, Jianwei, Chen, Youlo, Wang, Xiaoli, Pang, Liyun, Kong, Deling, Song, Bing, Li, Chen and Yang, Jing 2018. Nanoparticles with CD44 targeting and ROS triggering properties as effective in vivo antigen delivery system. *Molecular Pharmaceutics* 15 (2), pp. 508-518. 10.1021/acs.molpharmaceut.7b00890

Publishers page: [http://dx.doi.org/10.1021/acs.molpharmaceut.7b00890...](http://dx.doi.org/10.1021/acs.molpharmaceut.7b00890)

Please note:

Changes made as a result of publishing processes such as copy-editing, formatting and page numbers may not be reflected in this version. For the definitive version of this publication, please refer to the published source. You are advised to consult the publisher's version if you wish to cite this paper.

This version is being made available in accordance with publisher policies. See <http://orca.cf.ac.uk/policies.html> for usage policies. Copyright and moral rights for publications made available in ORCA are retained by the copyright holders.



Nanoparticles with CD44 targeting and ROS triggering properties as effective in vivo antigen delivery system

Xiaoyu Liang^a, Xuanling Li^a, JianweiDuan^a, Youlu Chen^a, Xiaoli Wang^a,Liyun Pang^a,
Deling Kong^{a,b}, Bing Song^c, Chen Li^{*a}, Jing Yang^{*a}

a. Tianjin Key Laboratory of Biomaterial Research, Institute of Biomedical Engineering, Chinese Academy of Medical Science and Peking Union Medical College, Tianjin 300192, China.

b. Key Laboratory of Bioactive Materials, Ministry of Education, Nankai University, Tianjin 300071, China.

c. School of Dentistry, College of Biomedical & Life Sciences, Cardiff University, Heath Park, Cardiff, CF14 4XY, UK.

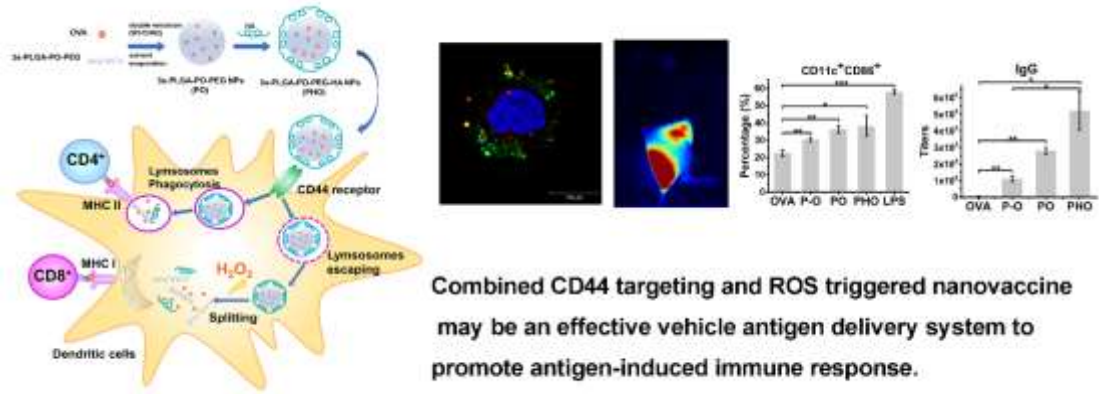
*Corresponding author: Prof Chen Li and Prof Jing Yang

Email address: yangjing37@hotmail.com; cli0616826@126.com

Mobile: 008613389060566; 008618920869998

Fax: 0086 022 87891191

Table of contents graphic



Abstract

Currently, development of subunit vaccine based on recombinant antigens or peptides has gradually become an important alternative option for traditional vaccine. However, induction of potent immune response with desired efficacy remains a major challenge. The nanoparticle-based antigen delivery system has been considered a potential carrier system to improve the efficacy of subunit vaccine. In the present study, we have designed an immune-stimulatory delivery system by conjugating three-armed PLGA to PEG via the peroxalate ester bond which is sensitive to hydrogen peroxide (H₂O₂), a major reactive oxygen species (ROS). Hyaluronic acid (HA), a ligand for CD44 receptors was also modified onto the outer shell of the 3s-PLGA-PEG nanoparticles to promote immune cell uptake. For in vitro and in vivo immune response assessment, a model antigen ovalbumin (OVA) was enclosed within the core of the 3s-PLGA-PEG nanoparticles to form 3s-PLGA-PO-PEG/HA nanoparticles (PHO NPs). Our results showed that the PHO NPs enhanced dendritic cell maturation, antigen uptake and antigen presentation in vitro, likely due to enhanced lysosomal escape. In vivo experiments further revealed that the PHO nanovaccine robustly promoted OVA-specific antibody production and T cell response accompanied by modest stimulation of memory T cells. In summary, the ROS-responsive PHO NPs with modified HA may be an effective vehicle antigen delivery system to promote antigen-induced immune response.

Keywords: ROS triggered; hyaluronic acid modified; nanoparticles; immune response

1 Introduction

Designing and preparation of appropriate delivery systems for biomacromolecules such as genes, proteins, polypeptides remains a major challenge in the field of drug delivery system development¹. The application of nanoparticles transferring system as vaccine carrier could potentially overcome limitations of subunit vaccines by increasing the antigen surface area, enhancing the stability of proteins, stabilizing the biological activity of antigens/proteins and augmenting the solubility of the antigen/protein complexes. Moreover, nanoparticles could prolong the systemic circulation time of antigens by processes such as encapsulation, which protects the active segments of antigens from endogenous enzyme degradation while promotes local accumulation. In addition, by employing nanoparticles as vaccine carriers, controlled and sustained release of antigens accompanied by other immune modulators can be achieved, which is essential to potent immune responses and lasting immune memory. In addition, studies have shown that nanoparticles can stimulate dendritic cell (DC) maturation and antigen presentation, both of which are crucial for the initiation of effective immune responses^{2, 3}. Moreover, -it has been shown that nanoparticles can stimulate immune responses, and that their compatibility with the immune system are mainly dependent on surface chemical reactivity of the nanoparticles. Reducing the immune toxicity of nanoparticles could make them useful platforms for drug delivery⁴.

Limited by their biological characteristics, biomacromolecules are easily degraded in vivo resulting in low bioavailability. As a result, for biomacromolecules delivery,

polymer nanocarriers have often been used⁵. However, while polymer nanocarriers improved bioavailability of the biomacromolecules, in vivo stability and toxicity have been reported with the use of liposomes and cationic polymers respectively. Instead, natural macromolecules have been shown to improve the distribution of nanoparticles in vivo with enhanced targeted delivery capability.

Hyaluronic acid (HA) is a natural protein polysaccharide and often found in the extracellular matrix and connective tissues. It plays an important role in the maintenance of extracellular matrix structure and regulation of intracellular activity. It also functions as ligand to CD44 receptor, a transmembrane glycoprotein which is one of the most important receptors on the cell surface. HA and HA receptor CD44 as well as the HA binding protein (e.g., hyaluronan⁶, proteoglycans and glycoproteins such as aggrecan, versican, neurocan or brevican) regulate a variety of biological behaviors of cells including cell adhesion, migration, proliferation, differentiation and wound healing⁷. Studies have shown that CD44 is highly expressed on cells such as tumor cells, dendritic cells (DCs) and some epithelial cells⁸. The binding of CD44 and HA can trigger the combination of CD44 cytoplasmic domain and signal transduction molecules and then induce and activate intracellular signal transduction pathways such as Rho/Ras signal⁹. Given the high level of expression of CD44 on tumor and DC surface, HA has been widely used during the construction of nanoparticles for targeted drug/antigen delivery¹⁰.

However, HA is easily degraded physiologically. When used alone as drug delivery system, it leads to reduced circulation time and drug leakage with decreased delivery

efficiency. Moreover, when inflammation occurs, certain enzymes can degrade HA derivatives, causing accidental drug release at the sites of inflammation¹¹. One previous study has been reported that polyethylene glycol (PEG) modification of HA could prevent HA degradation and increase HA stability in vivo, likely due to effective inhibition of plasma protein, enzyme and other substances adhesion on the surface by PEGylation¹². Thus, in the present study, we have designed a three-arm PLGA-PEG nanoparticle (3s-PLGA-PEG NPs) connected by peroxalate ester bonds as OVA antigen carrier, with HA modified on the external surface (3s-PLGA-PO-PEG/HA, PHO NPs). Since the peroxalate ester bonds are sensitive to ROS, which promotes in vivo immune responses and inflammation¹³, we expect that the PHO NPs would be able to target DCs by binding to the CD44 receptors while the ROS-responsiveness would enable targeted release of antigen for potent immune response induction.

2 Experimental section

2.1 Materials

D,L-Lactide(DLA) and GA were supplied by Glaco Ltd (Beijing, China). PEG (Mn = 4000 g/mol) wasbought from Guangfu Fine Chemical Research Institute (Tianjin, China). HA, Lipopolysaccharide(LPS), 3-(4,5-dimethyl-2-thiazolyl)-2,5-dipheny- 1-2-H-tetrazolium bromide(MTT), Phosphate Buffered Saline (PBS), Dimethyl sulfoxide (DMSO), Fluorescein isothiocyanate (FITC), 4',6-diamidino-2-phenylindole (DAPI), Tween 20 were obtained by Solarbio (Beijing,China). Ovalbumin(OVA), Polyvinyl alcohol(PVA) (Mn=30000-70000), Carboxyfluorescein diacetate, succinimidyl ester

(CFSE), 2,7-Dichlorodi -hydrofluorescein diacetate (DCFH-DA) were obtained from Sigma-Aldrich (St. Louis, MO, USA). Cyanine7 NHS ester was obtained by Apexbio (USA). The Micro BCA™ Protein assay kit was supplied by Thermo Fisher Scientific Inc. (Rockford, IL USA). Lyso Tracker Red was purchased from Beyotime Biotechnology (Shanghai, China). Roswell Park Memorial Institute (RPMI) 1640 and fetalbovine serum (FBS) were purchased from Gibco (Grand Island, NY, USA). Anti-mouse IgG Biotin, anti-mouse ELISA kits IL-6, TNF-alpha were purchased from eBioscience. Anti-mouse IgG1, IgG2a Biotin were obtained by BD biosciences. Recombinant mouse GM-CSF and IL-4 were purchased from Peprotech (Rocky, Hill, USA). Fluorochrome-labeled anti-mouse monoclonal antibodies (CD3e, CD28, CD4, CD8a, CD11c, CD40, CD86, MHCI, MHCII, CD44, CD62L) were purchased from eBioscience (CA, USA).

Female C57BL/6 mice(6-8-week-old) were purchased by National Institutes for Food and Drug Control (Beijing, China). All animal procedures were reviewed and ethically approved by Center of Tianjin Animal Experiment ethics committee and authority for animal protection (Approval No.:SYXK (Jin) 2011-0008).

2.2 Synthesis of 3s-PLGA-PO-PEG

The synthetic route of 3s-PLGA-PO-PEG was depicted as follow. The 3s-PLGA was firstly synthesized using lactide and glycolide by ring-opening polymerization as previously reported¹⁴. The block copolymer was obtained when modified 3s-PLGA and PEG linked with oxalyl chloride by acylation reaction. Three-arm PLGA connected to PEG by peroxalate ester bond which breaks in the presence of H₂O₂.

2.3 Preparation and characterization of NPs modified with HA

A double emulsion ($W_1/O/W_2$) method was used to prepare 3s-PLGA-PO-PEG/HA NPs loaded OVA (PHO). Firstly, OVA aqueous solution was added in 2 mL dichloromethane which containing 50 mg 3s-PLGA-PEG(LA:GA=50:50) to form water-in-oil (W_1/O) primary emulsion under a microtip probe sonicator (VCX-130-PB, Sonics & Material Inc., Connecticut, USA) at 30% amplitude for 10 min¹⁵. The first emulsion was then added in a secondary aqueous solution containing 1% (w/w) PVA with HA by ultrasonication at 30 % amplitude for another 10min to generate a $W_1/O/W_2$ double emulsion. The final preparation was stirred for 4 h and transferred into solid NPs until the dichloromethane completely removed. The HA-coated NPs were washed four times with distilled water by centrifugation at 23,000 rpm for 30 min before lyophilized and sterilized by gamma irradiation and stored at -20 °C in dry state and the supernatant was used to test loading capacity. The 3s-PLGA loaded OVA(P-O) NPs and 3s-PLGA-PEG loaded OVA (PO) NPs were also prepared as control in the same way. NPs loaded OVA conjugated FITC (OVA-FITC) or OVA conjugated Cy7 NHS ester(OVA-Cy7) were prepared using the above describe method for the purpose of tracking.

The average particle size, encapsulation and loading capacity and surface morphology were determined to evaluate the characteristics of NPs. The particle size, size distribution and surface charges of the NPs were determined by photon correlation spectroscopy (PCS)using Nano-ZS ZEN3600 (Malvern Instruments). Morphological test of NPs was measured and taken pictures by transmission electron microscopy (TEM, JEM-2100F, Japan). The NPs were suspended in water at 4°C over21 d and the

size was tested at different time to observe the size and distribution change of NPs. To determine the encapsulation efficiency (EE) and loading capacity (LC) of NPs, the amount of OVA in NPs and free OVA in supernatant were determined using BCA Assay Kit (Thermo, USA). The EE and LC calculated by the equations: $EE = (\text{total OVA} - \text{unbound OVA})/\text{total OVA} \times 100\%$; $LC = \text{loaded OVA}/\text{total mass of nanovaccine} \times 100\%$. The release kinetics experiment of NPs was carried out in phosphate buffer (PBS, pH 7.4) at 37 °C. 12 mg OVA-loaded NPs was suspended in PBS to release in shaking table at constant temperature (37 °C, 150 r/min). The release amounts of OVA from supernatant obtained by centrifugation (20000 r/min, 5 min) was measured at different time by BCA Assay Kit.

2.4 The scavenging ability of H₂O₂ by NPs in vitro

The scavenging ability of H₂O₂ by NPs was measured as follows. To 1 mL of H₂O₂ solution (200 μM) was added 1 mg of polymer materials, P-O, PO, PHO NPs and free OVA and then was left in a shaker (150 r/min) at 37°C. The H₂O₂ concentration of supernatant was measured after 3 h incubation by Amplex Red Probe (Invitrogen, Carlsbad, CA). Human smooth muscle cells (SMC) were cultured with 1 μg/mL LPS to induce intracellular ROS in a 24-well plate and then treated with NPs for 3 h. Then, ROS in cells was labeled by 10 μmol/L DCFH-DA. The fluorescence signal of ROS in cells was measured using a BD Accuri™ C6 flow cytometer (BD Biosciences, San Jose, CA).

2.5 Dendritic cells viability assays

To evaluate the potential cytotoxicity of NPs on cells, we performed a MTT assay of

cells treated with soluble OVA or NPs. DC 2.4 cells were cultured in RPMI1640 with 10% FBS, 100 µg/mL penicillin, 100 µg/mL streptomycin under 5% CO₂ at 37°C. They were seeded in 96-well plates in 100 µL medium per well at a density of 5×10^4 cells/mL for 24 h and then cells were washed and incubated for another 24 h with 100 µL of medium-containing free OVA or NPs. Then, the NP-containing medium was removed. 0.5mg/mL MTT solution in medium was added and kept for 4 h. At last, the supernatant was removed and 150 µL DMSO was added. Cells were covered with tinfoil and agitated on orbital shaker for 15 min. Absorbance was read at 490 nm with a reference filter of 630 nm using a microplate reader (Varioskan Flash 3001, Thermo, USA).

2.6 Intracellular uptake of OVA by DC

DC 2.4 cells were firstly cultured at 5×10^5 cells/well in a 24-well plate for 24 h and then treated with OVA-FITC (10 µg/mL) and nanoparticle-formulated OVA-FITC at 37 °C for 4 h and then washed. The uptake percentage and mean fluorescence intensity(MFI) of OVA-FITC by DCs was measured by a BD Accuri™ C6 flow cytometer (BD Biosciences, San Jose, CA).

2.7 Cellular uptake and localization of antigens in DC

DC 2.4 cells were seeded in cover glass-bottom confocal dish at a density of 8×10^4 cells/well overnight at 37 °C. Free OVA-FITC (10µg/mL) and OVA-FITC loaded NPs were placed in wells and incubated at 37 °C for 4 h. The cells were washed for three times and then were fixed with 4% paraformaldehyde. The 50nM LysoTracker Red DND-99 and DAPI was separately used to label endosomes and nucleus. The fluorescent images were recorded by a confocal laser scanning microscopy (CLSM 410;

Zeiss, Jena, Germany)

2.8 Bone marrow dendritic cells (BMDCs) stimulation and maturation

BMDCs which were isolated from C57BL/6J mice femurs and tibias. Erythrocytes were lysed by red cell lysing reagent. BMDCs were then cultured in complete RPMI1640 medium containing 20 ng/mL GM-CSF and 10 ng/mL IL-4 for 6 d to obtain immature DCs¹⁶. The immature DCs were treated with free OVA (20 µg/mL) and OVA-loaded NPs for 24h. The levels of surface markers expression were observed by flow cytometry. The DCs were stained with anti-mouse CD11c, CD40, CD86 and CCR7 monoclonal antibodies for 30 min at 4 °C in the dark. Cells were washed twice and then analyzed by flow cytometry using a BD Accuri™ C6 flow cytometer (BD Biosciences, San Jose, CA).

2.9 Antigen cross presentation in vitro

In vitro antigen cross presentation by DCs was evaluated by B3Z T cell activation assay¹⁷. Immature BMDCs were harvested and pulsed with free OVA or OVA loaded NPs in a 24-well plate for 8 h at 37 °C. BMDCs were washed and then cocultured with B3Z T cells at a density of 5×10^5 cells/well which is the CD8⁺ T cell hybridoma presented by MHC class I molecules overnight. X-Gal substrate (1.5 mg/mL of X-Gal, 0.25% PBS-NP40) was added to the remaining cells and then incubated for 24 h. Finally, the positive signal was measured by a microplate reader (Thermo) at 405 nm.

2.10 In vivo trafficking of cyanine 7-labeled NPs

To investigate the effect of nanovaccines on lymphatic trafficking in vivo, OVA was labeled by near infrared (NIR) fluorescent Cyanine 7 dyes. C57BL/6 mice were

administrated by subcutaneous (s.c) injection at the tail base site and OVA-Cy7 and OVA-Cy7 NPs were then visualized at the injection site and the inguinal lymph nodes¹⁸. Cy7 fluorescent signals at different time (0, 6, 12, 24 h) was measured by Maestro imaging system (CRI, USA). Fluorescence quantitative change was measured by quantifying the fluorescent intensity.

2.11 In vivo immunization, antibody production and in vitro T cell proliferation assay

Six-to-eight-week-old female C57BL/6J mice (4 mice/group) were immunized with OVA or OVA-loaded NPs (20 µg OVA/mouse) by subcutaneous injection at a 2-week interval for three times. As for antibody production analysis, blood was collected 7 days after last immunization, OVA specific IgG, IgG1, IgG2a antibody in serum were determined by ELISA (eBioscience).

Seven days post last immunization, splenocytes (1×10^6 cells/mL) were isolated and stimulated with OVA (20 µg/mL) in a 24-well plate for 72 h. The production of IL-6 in supernatants was measured by ELISA kit. To determine T lymphocytes proliferation, splenocytes were isolated and stained with 5 µmol/L CFSE (Sigma-Aldrich). After anti-mouse CD3 and anti-mouse CD28 immobilized in a 24-well plate, the CFSE-dyed T cells (1×10^6 cells/mL) were incubated with 20 µg/mL soluble OVA for 72h. Finally, the cells were labeled with PE-anti-mouse CD4 or PE-anti-mouse CD8, and decreased CFSE intensity was determined to observe different T cell proliferation using flow cytometry.

2.12 T cell activation response in vivo

Six-to-eight-week-old female C57BL/6J mice were immunized with OVA (20 µg/mL) or OVA loaded NPs twice every two weeks. Splenocytes (1×10^6 cells/mL) were isolated and cocultured with OVA (20 µg/mL) for 72 h at 37 °C. Cell surface markers FITC-anti-mouse CD62L, APC-anti-mouse CD44, PE-anti-mouse CD4 or PE-anti-mouse CD8 were stained. Fluorescence populations were sorted using a BD Accuri™ C6 flow cytometer (BD Biosciences, San Jose, CA) to measure the amount of effector memory T cells ($CD44^{Hi} CD62L^{Lo}$) and central memory T cells ($CD44^{Hi} CD62L^{Hi}$)¹⁹.

2.13 Statistical analysis

The quantitative data were presented as mean \pm S.D. Statistical significance were analyzed using a student's T-Test (*P<0.05; **P<0.01; ***P<0.001).

3 Results and discussion

3.1 Characterization of NPs

NPs were prepared by a double emulsion ($W_1/O/W_2$) solvent evaporation method. Soluble OVA were added in PLGA or PLGA-PEG organic phase to form W_1/O primary emulsion. The emulsion was then emulsified in PVA with HA to multiple emulsion ($W_1/O/W_2$). Due to the binding affinity of HA to CD44 receptors, we expect that the PHO NPs would be readily taken up by antigen-presenting cells (APCs), such as DCs, following recognition of CD44 receptor on APCs cell surface. Since uptake of foreign particles would activate the NADPH-oxidase which catalyzes the glycolytic reactions and results in H_2O_2 generation, the ROS-responsive NPs would then degenerate in an H_2O_2 -rich environment within DCs due to breakage of the peroxalate ester bonds,

leading to release of antigen within the NPs.

Table 1. Characteristics of OVA-loaded P-O, PO, PHO. Data are shown as the mean±SD (n=3).

NPs	Size(nm)	PDI	Zeta potential(mV)	EE	LC
P-O	219.3 ± 0.82	0.144 ± 0.016	-19.9 ± 0.3	15.2 ± 0.8	3.6 ± 0.2
PO	200.0 ± 2.43	0.270 ± 0.003	-22.0 ± 1.4	85.0 ± 11.1	12.5 ± 0.9
PHO	225.0 ± 1.29	0.097 ± 0.034	-7.27 ± 0.4	94.4 ± 2.1	15.4 ± 0.3

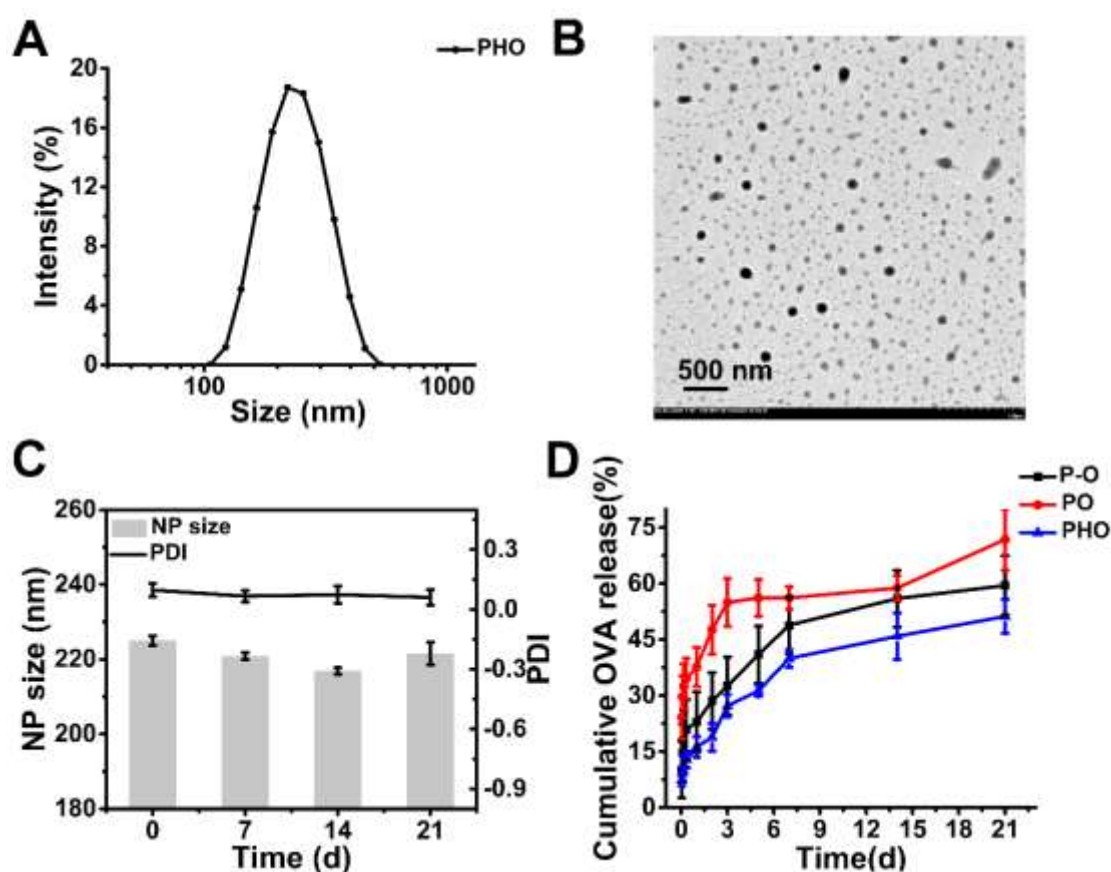


Fig. 1 The physical properties of NPs in vitro. (A) PHO size distribution. (B) TEM image of PHO. (C) The change of PHO particle size and PDI for 21 d was measured to observe the stability of particles. (D) The release kinetics curve of P-O, PO, PHO in

PBS (0.01 M, pH 7.4) for 21d. Data are mean \pm SD (n=3).

Thus, OVA loaded 3s-PLGA-PO-PEG/HA (**PHO**) NPs, 3s-PLGA (**P-O**) NPs and 3s-PLGA-PO-PEG (**PO**) NPs were prepared. The average diameter of PHO NPs was 225.0 ± 1.29 nm and polydispersity index (PDI) was 0.097 ± 0.034 . The size distribution of PHO NPs was presented in Fig. 1A. The surface charge of PHO NPs was -7.27 ± 0.4 mV (Table 1). The results of TEM and Dynamic Light Scattering showed that all groups of NPs exhibited dispersed spherical shape of similar size (Fig. 1B).

The protein capsulation efficiency (EE) and loading capacity (LC) were listed in Table 1. We found that PEGylation increased OVA loading likely due to the hydrophilicity of PEG. In addition, HA modification also increased viscosity of NPs and protein adhesion. The stability of the NPs was then investigated. Our results observed no evident morphological changes of all groups of NPs for 21 days at 4 °C, indicating suitable stability of the NPs (Fig. 1C).

It has been demonstrated that PEG fragments not only increase the stability of NPs, but also reduce proteolysis, both of which result in increased circulation time and improved efficacy²⁰. Since HA is a member of the mucopolysaccharide family with high viscosity that may attenuate protein release, we have also examined the protein releasing ability of the NPs (Fig. 1D). We observed sustained OVA release from all OVA-loaded NPs in PBS (pH 7.4) for 21 days. A burst release of more than 20% was detected during the first day for P-O and PO, followed by a slower and continued release for 20 days. In contrast, OVA were released from the PHO NPs in a slower manner compared to the P-

O and PO groups, mainly due to the viscosity of the HA coatings.

Given that smaller particles (20-200 nm) tend to accumulate within the LN-resident DCs and other monocytic APCs²¹, our NPs could potentially be effective nanovaccine delivery vehicles considering their narrow size distribution, high encapsulation efficiency, stability and sustained antigen-releasing property.

3.2 Hydrogen peroxide responsiveness of NPs in vitro

It has been known that the peroxy oxalic ester bonds, which connect the PLGA and PEG segments of the 3s-PLGA-PO-PEG NPs, are sensitive to H₂O₂. In the presence of H₂O₂, breakage of the PO bonds would lead to degeneration of the NPs. To assess the responsiveness and the scavenging H₂O₂ property of the NPs by the amplex red hydrogen/peroxidase assay²². As shown in Fig. 2A, the concentrations of remaining H₂O₂ detected from PO or PHO NPs were fewer in comparison to P-O NPs and PEG solution. To further examine the H₂O₂ clearance action of the ROS-responsive NPs, human fibroblast NIH 3T3 cells were treated with NPs. ROS was labeled with DCFH-DA probe and quantified using flow cytometry. We observed reduced H₂O₂ levels from cells treated with soluble OVA, P-O, PO and PHO NPs compared to control cells (Fig. 2B). Cells treated with PHO NPs showed the most substantial decrease of ROS than cells treated with OVA or P-O, demonstrating better ROS scavenging ability of the PHO NPs.

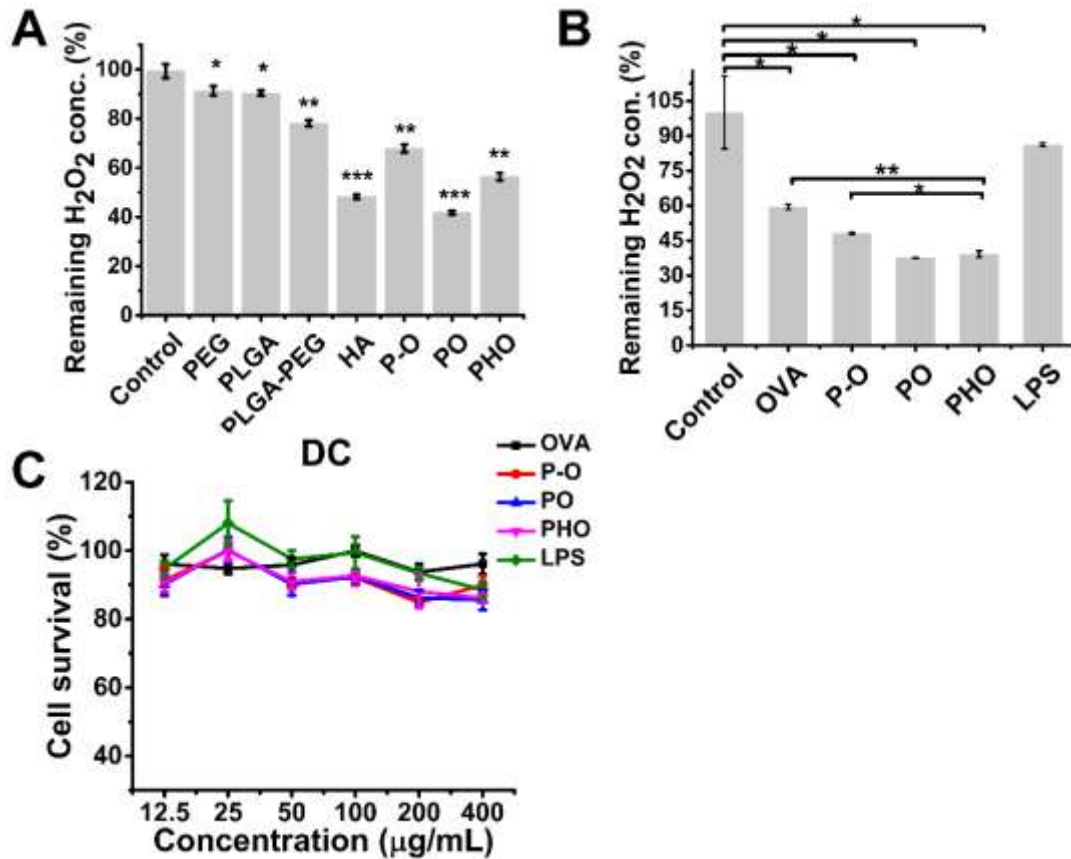


Fig. 2 H₂O₂ scavenging of NPs in vitro. (A) Scavenging activity of polymer materials and NPs determined by the Amplex Red Assay. (B) Scavenging of H₂O₂ by NPs in cells determined by a DCFH-DA probe. (C) Cytotoxicity of NPs for DC2.4 cells after 24 h determined by the MTT assay. The values shown are mean \pm SD (n=3). *P < 0.05, **P < 0.01 and ***P < 0.001 to control.

3.3 In vitro stability and toxicity of NPs

To determine in vitro stability and toxicity of the NPs, cell viability was assessed using a dendritic cell line (DC 2.4). Cell viability was performed using the MTT assay after cells were treated with a series of NPs ranging from 12.5 µg/mL to 400 µg/mL. Cell viability was calculated as follows: cell viability% = (sample OD - blank OD) / (negative control OD - blank OD) \times 100%. As shown in Fig. 2C, DC 2.4 cells exposed to all groups of NPs exhibited robust viability. The results demonstrated that NPs

composed of PLGA, PEG, HA exhibited excellent in vitro biological compatibility and are suitable as vaccine delivery vehicles.

3.4 NPs enhanced antigen uptake, DC maturation and cross-presentation

Antigens are initially processed by APCs, such as DCs and macrophages. These cells then regulate subsequent immune responses via antigen presentation of processed antigens to T or B cells. The potency of immune responses, as a result, is dependent on efficacy of antigen presentation of APCs following antigen uptake. Since HA bind to CD44 receptors on surface of cells such as DCs, the PHO NPs would enable targeted antigen delivery and uptake, which would be expected to increase efficiency of antigen presentation. We therefore have investigated the effect of all groups of NPs on antigen uptake, DC maturation and cross-presentation using the model antigen OVA uptake and localization of OVA-FITC was examined by confocal fluorescent microscopy (Fig. 3A) in DC2.4 cells. The images showed that soluble OVA-FITC and P-O NP groups was co-localized with lysosomes (shown in red) and the green fluorescence which corresponds to OVA-FITC was rather faint, indicating low level of free OVA uptake. Compared with soluble OVA, we observed more intense green fluorescence signal that indicates elevated intracellular OVA in cells treated with PO and PHO NPs. In cells treated with PO and PHO NPs, majority of OVA uptake was detected in the cytosolic space separated from lysosomes, demonstrative of “lysosomal escape” of the antigen and possible cross-presentation downstream.

The exact amounts of OVA-FITC uptake by DCs treated with different groups of NPs were quantified by measuring the mean fluorescence intensity (MFI) of FITC via flow

cytometry. As shown in Fig. 3B, an over 10-fold increase of OVA-FITC uptake was observed in DCs co-cultured with PHO NPs in comparison to OVA control group. Similar pattern was also observed in the MFI of OVA-FITC uptake (Fig. 3C). These results indicate that HA could enhance antigen recognition and internalization by DCs, possibly via its binding to CD44 receptors. In addition, we also observed increased OVA-FITC uptake from cells treated with PO NPs in comparison to P-O, which suggest PEGylation also improve antigen uptake. Moreover, since antigens uptake promotes a host of intracellular ROS production in cells. Our ROS-responsive NPs would further target to immune cells following phagocytosis of OVA.

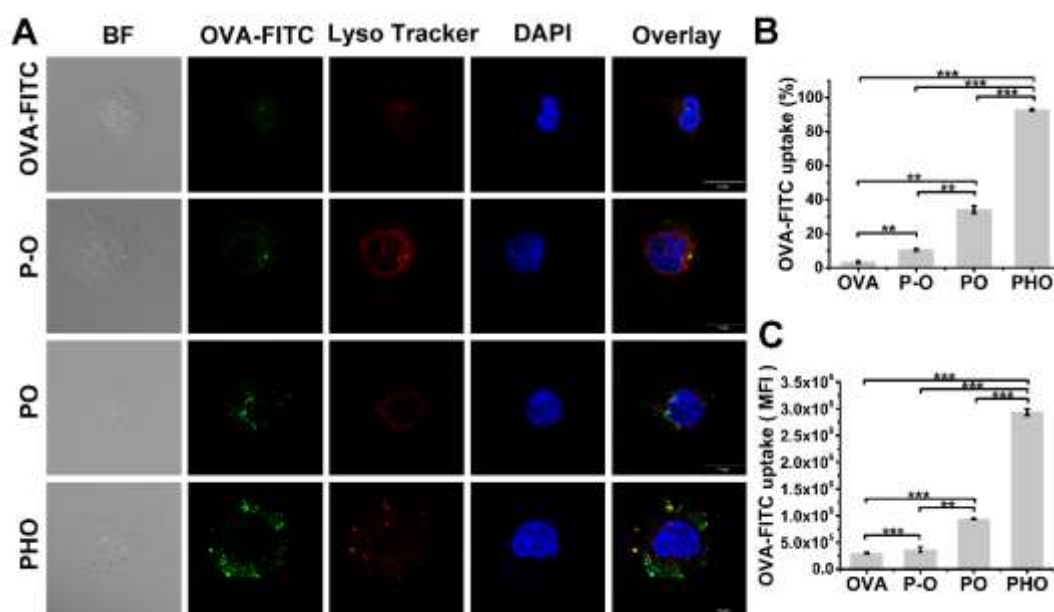


Fig. 3 Cellular uptake and endosomal release of NPs by DC2.4 cells. (A) Confocal microscope images of DC2.4 cells after incubated with soluble OVA-FITC and OVA-FITC NPs for 3 h. The scale bar shows 20 μ m. (B) The percentage of OVA-FITC uptake was determined by flow cytometry. (C) The intracellular MFI of DC 2.4 cells cocultured with soluble OVA-FITC and OVA-FITC NPs for 3 h was detected by flow cytometry. Bars shown are mean \pm SD (n=3). *P < 0.05, **P < 0.01 and ***P < 0.001 to OVA

groups.

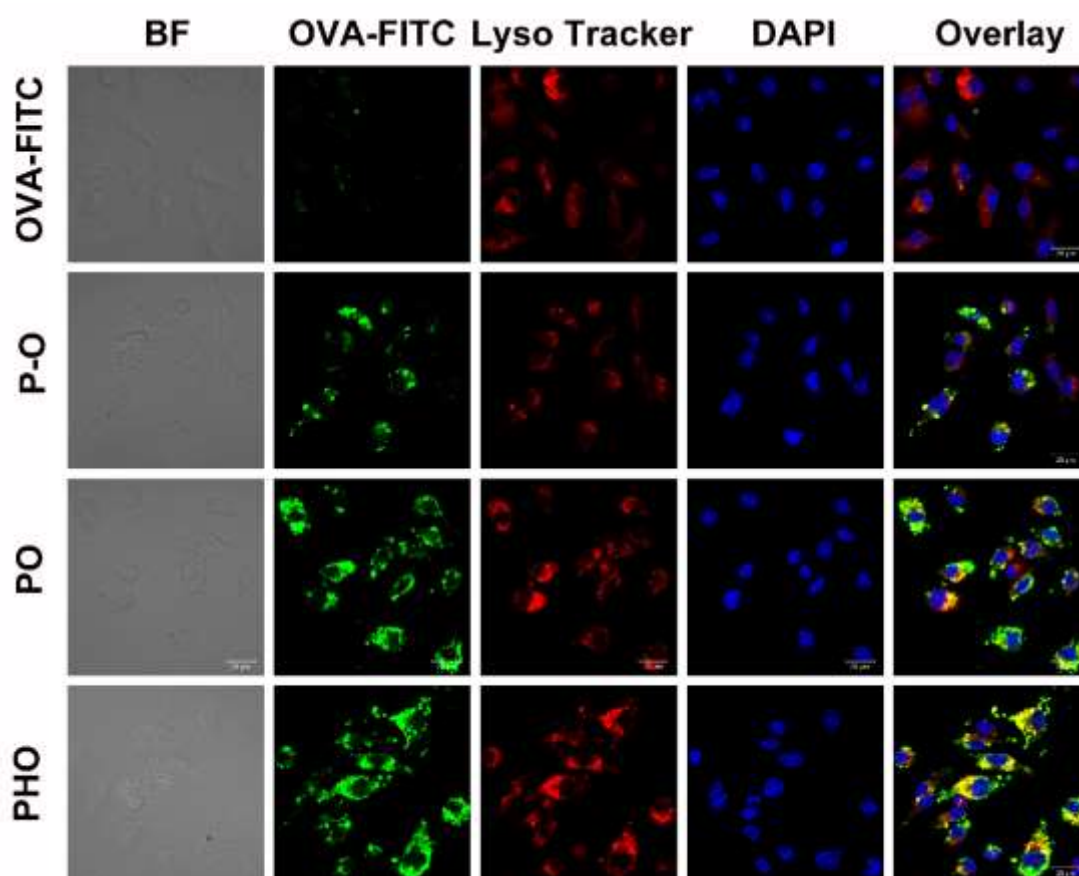


Fig. 4 Cellular uptake and endosomal release of NPs by BMDC cells. Confocal microscope images of BMDC cells after incubated with soluble OVA-FITC and OVA-FITC NPs for 3 h. The scale bar shows 20 μ m.

Dendritic cells play an essential role in antigen presentation and vaccine induced adaptive immunity. The recognition and antigen uptake by immature DCs is the first process during induction of immune responses. Following antigens uptake, DCs would undergo and become ready for subsequent processing of the antigens and presentation to T cells, a stage often referred to as maturation and characterized by up-regulation of

costimulatory molecules (such as CD40 and CD86) on matured DC cell surface. Since DC maturation is critical to T cell and immune response activation, we have further investigated the effect of NPs on DC maturation in vitro using bone marrow derived DCs (BMDCs). Thus, immature BMDCs were harvested on day 7 and exposed to NPs for 24h. Both PO and PHO NPs enhanced the expression of CD40 and CD86 (Fig. 5A, B), indicating their capability of promoting DC maturation.

Antigen cross-presentation is another step following antigen uptake and DC maturation, during which DCs present the processed antigens to CD4⁺ or CD8⁺ T cells through the MHC class II or MHC class I pathways, respectively. To measure the effects of NPs on antigen presentation, BMDCs were pulsed with free OVA or NP-formulated OVA for 24 h, and co-cultured with OVA-responsive B3Z T cells hybridoma overnight. Indeed, the LacZ B3Z T cells are sensitive to OVA class I epitope SIINFEKL that is known to be presented by the MHC class I H-2Kb on DCs and are able to generate β -galactosidase upon antigen recognition, concentrations of β -galactosidase were quantified from all tested groups²³. As shown in Fig.5C, P-O NPs significantly enhanced the value of OD 405 by 2folds compared to free OVA, indicating OVA-specific CD8⁺T cell activation. PO and PHO NPs also induced significantly elevated CD8⁺T cell activation than free OVA. It has been known that endogenous antigens are often presented via the MHC class I pathway, while exogenous antigens are presented via the MHC class II pathway²⁴. Since our results showed up-regulation of CD8⁺ T cell activation following exposure to NP-delivered OVA, it could be said that NPs promoted antigen cross presentation possibly due to enhanced DC phagocytosis, antigen release and lysosomal

escape that had been observed with the ROS-responsive NPs. Cytokine release by mature DCs is also important for the induction of local immune responses. We have also measured cytokine productions in supernatants of BMDCs that had been co-cultured with NP-delivered OVAs. As shown in Fig. 5D, E, BMDCs secreted significantly more IL-6 and TNF- α following NPs stimulation compared to free OVA, consistent with a pro-inflammatory role of the NP-delivered OVAs.

Our results indicate that NPs promoted antigen uptake, DC maturation and cross-presentation, accompanied by pro-inflammatory cytokine production compared to free OVA. However, no significant differences could be detected among different composition of the NPs, which could mean that the PLGA NPs themselves were a potent adjuvant. Indeed, previous studies have reported adjuvant property of PLGA, consistent with our results²⁵.

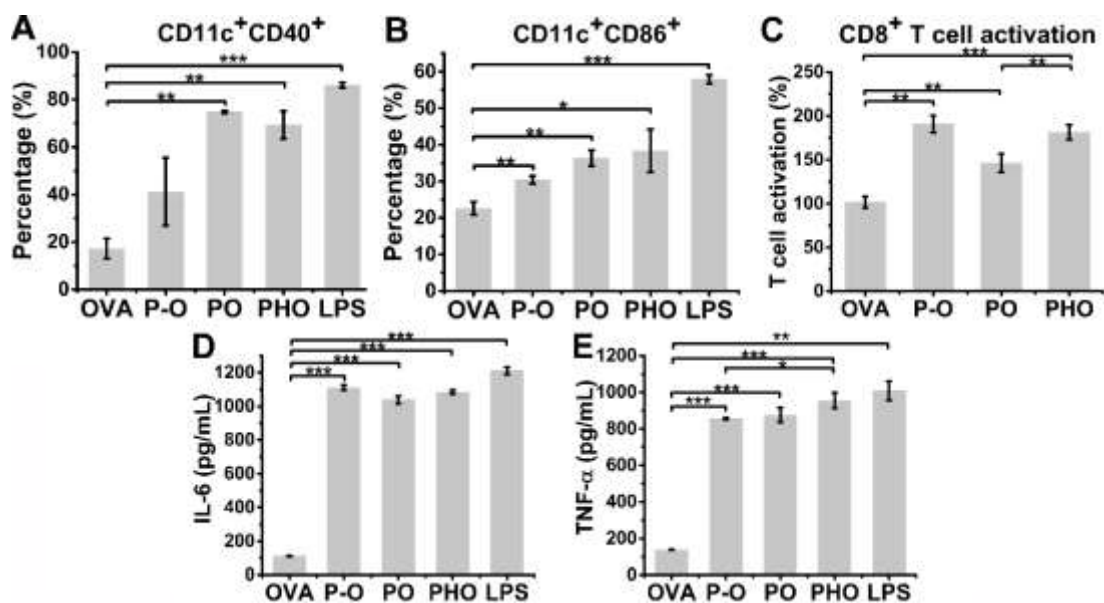


Fig. 5 BMDCs maturation and cytokine production induced by free OVA or NPs cocultured for 24 h in vitro. (A, B) The expression of CD40 and CD86 on BMDCs was

determined using flow cytometry. (C) MHC I antigen presentation by BMDCs to B3Z cells to observe CD8⁺T cell activation in vitro. (D, E) The secretion of IL-6 and TNF- α from BMDCs with different NPs. The values were mean \pm SD (n=3). *P < 0.05, **P < 0.01 and ***P < 0.001 to soluble OVA.

3.6 Nanovaccine enhances antigen in vivo trafficking

As an important immune organ, lymph nodes will uptake antigen by DCs or macrophages to activate immune response. Antigens are expected to migrate to the draining lymph nodes and NP in vivo trafficking has been used as an indicator to monitor vaccine delivery. It has been reported that smaller particles were more often found in lymph nodes while larger particles were more efficiently phagocytosed by DCs²⁶. As a result, considering that the NPs used in the present study range less than 200 nm, we expect that they would be readily transferred to lymph node following administration. To assess the effect of NPs on migration properties, fluorescently labeled OVA (OVA-Cy7) and NPs-delivered OVA-Cy7 were injected by subcutaneously at the tail base site and in vivo trafficking of OVA-Cy7 was monitored by examining the fluorescence signal of Cy7 using a small animal in vivo imaging system.

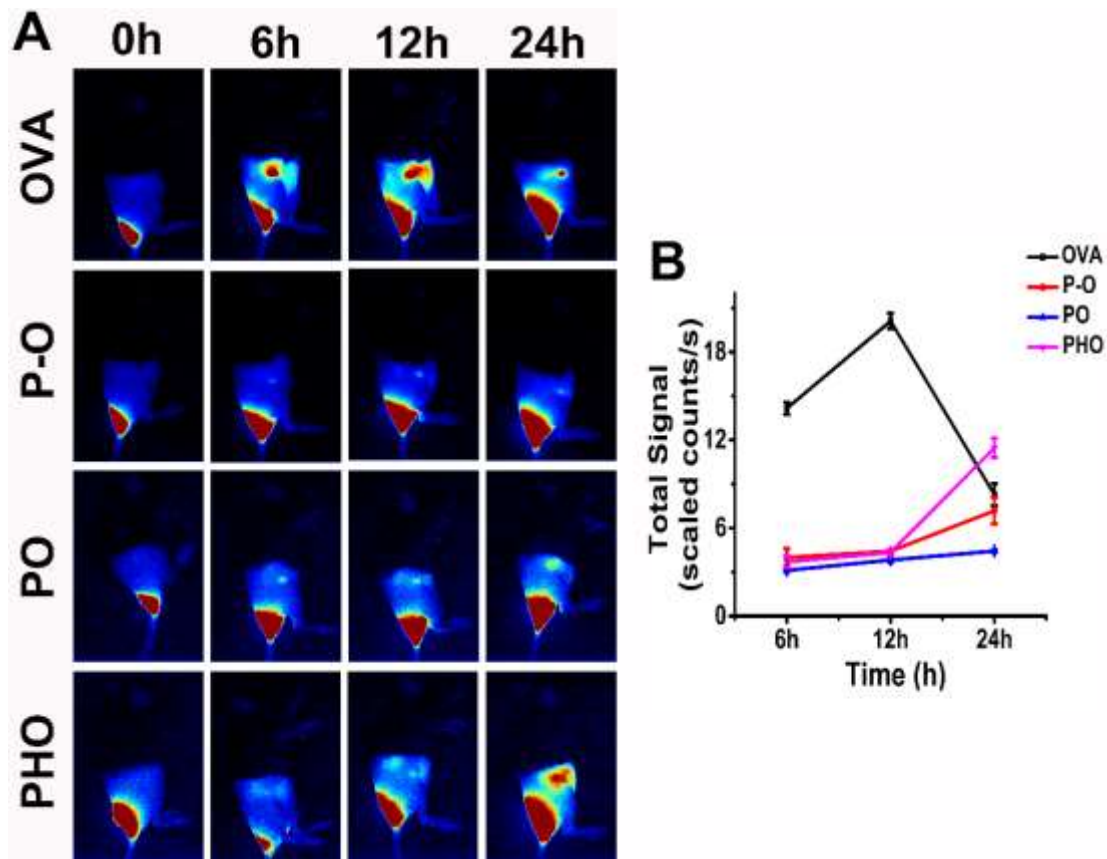


Fig. 6 Antigen persistence at injection sites and transport into the right inguinal draining lymph node to determine in vivo tracking of OVA-Cy7 and OVA-Cy7 NPs. (A) Fluorescence images of different NPs in mice. (B) The total signal intensity of antigen in the right draining lymph node was calculated.

As shown in Fig. 6A, significantly strong fluorescence signals were observed in the inguinal draining lymph node at 6 h from mice received free OVA, and the signals increased at 12 h followed by a rapid decrease 24 h after injection. In contrast, the fluorescence signals of mice received P-O, PO, PHO NPs migrated slowly and the residence time in lymph nodes was prolonged compared to free OVA. The fluorescence signals detected in lymph nodes of all NPs group became stronger 12 h after initial administration. For mice received PHO NPs in particular, robust fluorescence signal was detected at 24 h (Fig. 6B), which could be due to increased DC targeting property

of the NPs as a result of HA modification. We also monitored the fluorescence signals for more than 1 week with attenuated fluorescence intensity detectable as time extended. Nevertheless, we found that administration of NPs would result in slow accumulation and retention of OVA in the LNs compared to soluble OVA (Fig. S1).

3.7 Nanovaccine enhanced in vivo T cell activation and antibody production

Six-week old female C57BL/6J mice were immunized with OVA or OVA-loaded NPs (20 μ g OVA/mouse) as detailed in the Methods section. Splenocytes were then isolated 7 days after the last immunization and labeled appropriately as previously reported for T-cell proliferation study²⁷. We found that mice immunized with PO and PHO NPs had elevated numbers of spleen CD8⁺ T cells than other groups (Fig. 7A, B). Up-regulation of CD4⁺ T cell number was also observed in mice treated with PO NPs (Fig. 7A). As shown in Fig. 7C, D, increased percentages of both CD4⁺CFSE^{low} and CD8⁺CFSE^{low} T cells were observed in all NP groups compared to free OVA. Since T cell proliferation is a key indication of immune activation, these results implicate a stimulatory role of NPs on both CD4⁺ and CD8⁺ T cells proliferation and immune activation. However, administration of PHO nanoparticles did not increase T-cell proliferation or activation in vitro, which could be due to the lack of memory T/B cell and circulating cytokines signaling system in a simplified in vitro environment. The aim of vaccine design is to induce adaptive immune response, i.e. cellular or humoral immunity. In general, antigen presenting cells (APC), including DCs, mononuclear / macrophages, are part of the innate immune system and are the first line of defense during pathogen invasion. The antigens can be identified and transported locally by the DCs from the infected

peripheral tissues or transferred systemically to the lymph nodes for further processing. DCs stimulate the response of T cells to antigens, usually by the pattern recognition receptor (PRR) to identify the immunogenic components. The commonly acknowledged PRRs are Toll like receptors and mannose receptors. The Toll like receptors recognize a variety of bacteria and viruses. Following PRR identification on DC surface, the pathogen / antigen is usually taken in by the DC through endocytosis / phagocytosis. When the antigen enters APCs such as DCs, it is then presented by MHC- I or MHC- II molecules. Exogenous particles, viruses, or pathogens are usually processed into small molecular antigens and then packed into the MHC- II molecules. The MHC- II presentation pathway then initiates the activation of auxiliary T cells, which further stimulates the production of antibodies or cellular immunity. On the other hand, the MHC- I presentation pathway is often activated through endogenous antigens within the cytoplasm of DCs. Together, the MHC- I and II presentation is known as cross presentation. Ultimately, the antigen presentation process triggers downstream signaling protein (cytokine) activation and induce adaptive immunity of the auxiliary T cells (Th cells). Taken all the above into consideration, the PLGA-based nanovaccine carriers are likely able to induce cellular immune responses and Th1 immune responses in vivo as observed in previous and our present study^{3, 28, 29}.

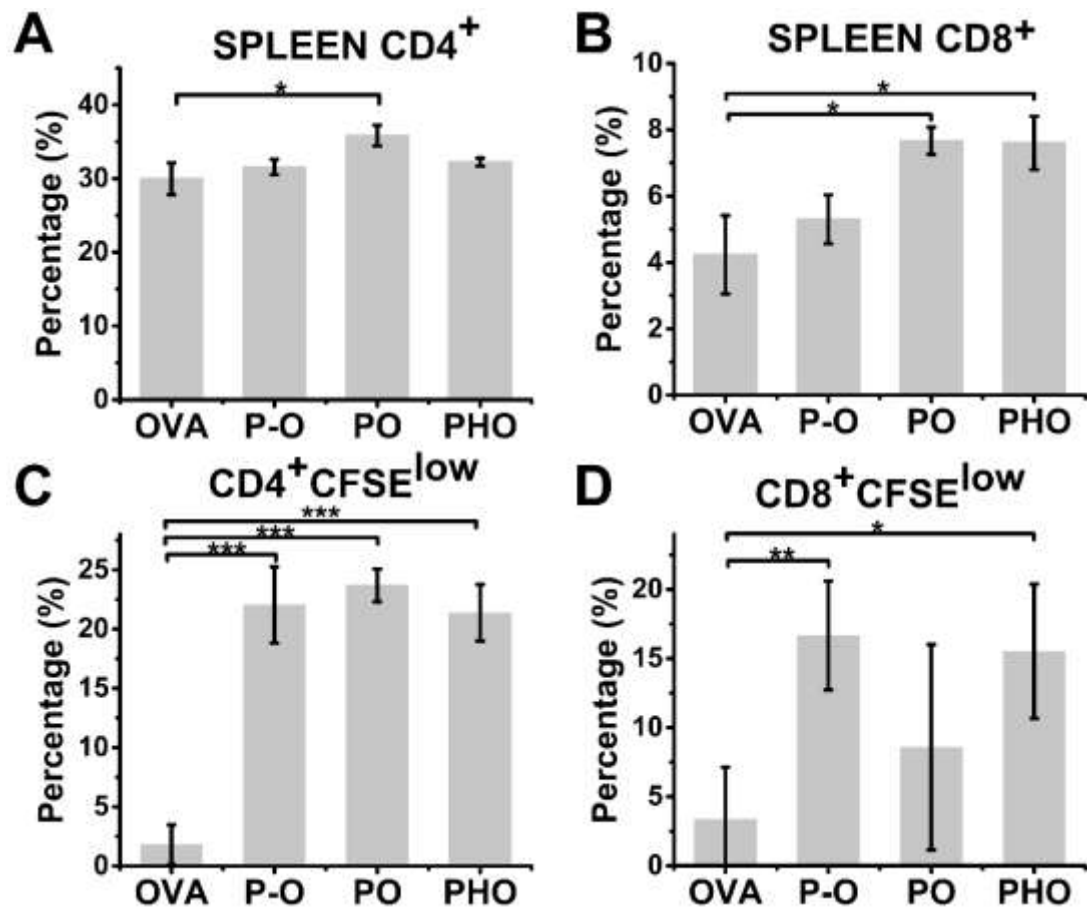


Fig. 7 Effect of NPs on promoting T cell proliferation and MHC I and II antigen presentation pathway. (A, B) CD4⁺ and CD8⁺ T cells were obtained and restimulated with OVA from immunized mouse splenocytes isolated 7days after last immunization. (C, D) The percentage of CFSE low proliferated CD4⁺ and CD8⁺ T cells labeled with CFSE, PE-anti-mouse CD4 or PE-anti-mouse CD8 was determined with decreased CFSE intensity using flow cytometry. The values are mean \pm SD (n=3). *P < 0.05, **P < 0.01 and ***P < 0.001 to OVA group.

To determine humoral immune response in vivo, C57BL/6J mice were immunized with OVA or OVA-loaded NPs, and anti-OVA IgG antibodies were measured 7 days post last immunization. As shown in Fig. 8, P-O and PO NPs induced anti-OVA specific IgG by 10-30 folds, meanwhile PHO NPs increased IgG production by 50 folds. We also measured anti-OVA IgG1 and IgG2a levels. The PHO NPs enhanced OVA-specific

IgG1 and IgG2a production more than other NPs and free OVA. It is known that in mice, Th1 T cell activation will often produce IgG2a antibody whilst Th2 T cell activation would likely induce IgG1 antibody generation³⁰. As a result, since elevation of both IgG2a and IgG1 antibodies was observed, the PHO NPs would likely promote both Th1 and Th2 cell immune response in vivo. In addition, elevated IL-6 production was also observed in splenocytes extracted from mice treated with PHO NPs, confirming a potent role of the PHO NPs in promoting immune cells proliferation, differentiation and CTL response induction.

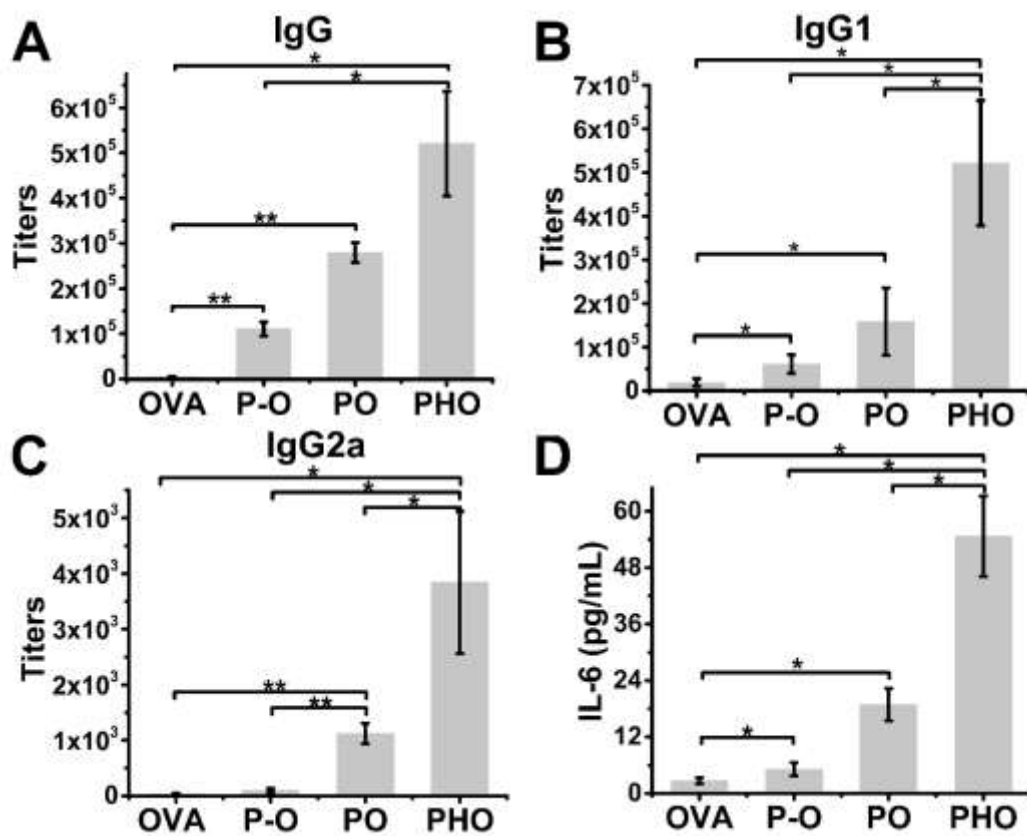


Fig. 8 Antigen-specific antibody production in the C57BL/6 mice immunized with OVA or OVA-loaded nanoparticles. (A-C) OVA specific IgG, IgG1, IgG2a titers in serum were measured using ELISA. (D) The secretion of IL-6 in supernatants was measured from splenocytes isolated after immunization and re-stimulated with soluble OVA for

72h. The values are mean \pm SD (n=3). *P < 0.05, **P < 0.01 and ***P < 0.001 to soluble OVA.

3.8 Nanovaccines enhanced memory T cell proliferation in vivo

Memory T cell responses were measured by lymph node homing receptors. According to the difference of expression of lymph node homing receptors, memory T cells are divided into effector memory T cells (CD44^{Hi} CD62L^{Lo}) for rapid effector function and central memory T cells (CD44^{Hi}CD62L^{Hi}) for potent proliferation and lymph node homing properties^{31, 32}. As shown in Fig. S2, the PHO NPs improved central memory T cells proliferation in both CD4⁺ T cells compared to other NPs. However, there was no significant difference from all groups in effector memory T cells, which may due to the effective cells gathering in central lymphoid organ.

4 Conclusions

In the present study, we have designed a ROS-triggered 3s-PLGA-PO-PEG nanoparticle-based antigen delivery system with HA modification that targets the CD44 receptors on DC surface (PHO NPs). We found that the PHO NPs enhanced dendritic cell maturation, antigen uptake, lysosomal escape and antigen presentation in vitro. PHO NPs also robustly promoted OVA-specific antibody production while stimulated antigen-induced both CD4⁺ and CD8⁺ T cell responses as well as memory T cells (Fig.9). In summary, the ROS-triggered nanoparticle-based antigen delivery system could enhance vaccine-induced cellular and humoral immune responses and may be a promising candidate as a novel vaccine.

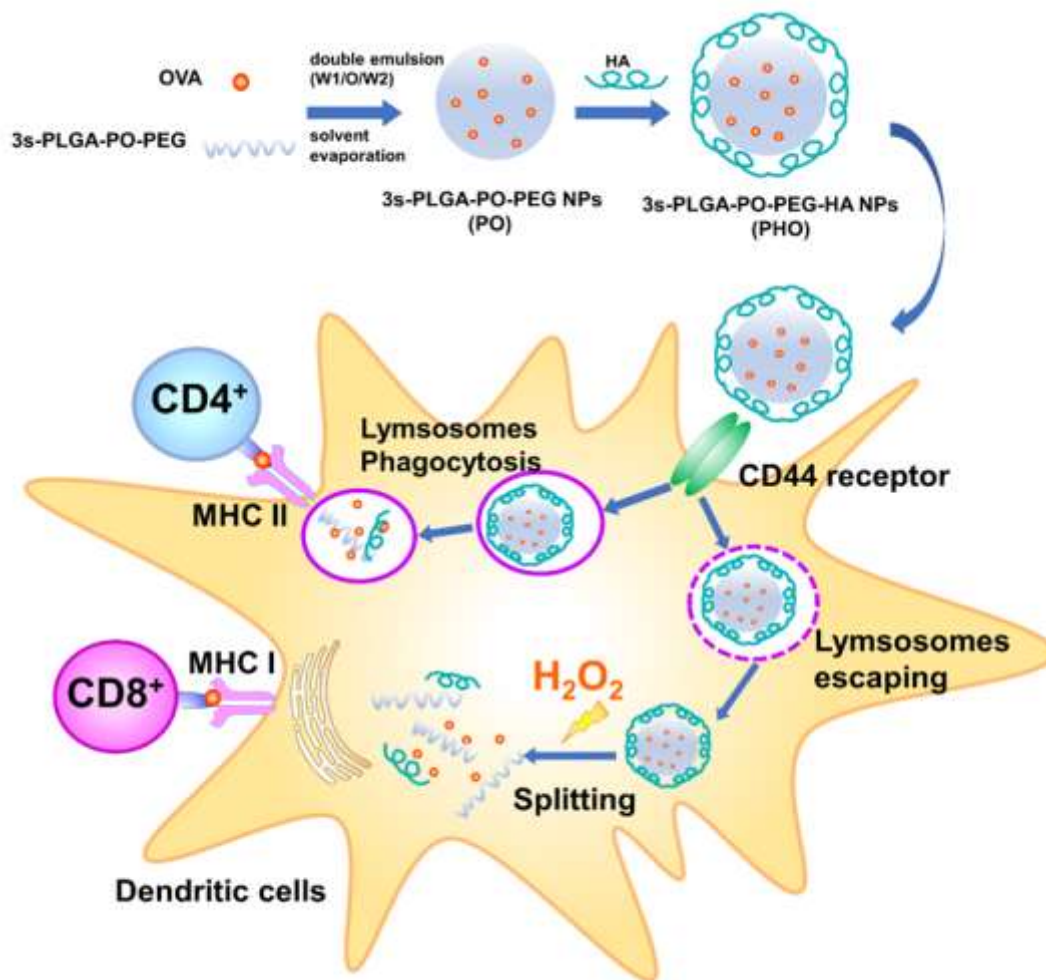


Fig. 9 The design of nano vaccine and possible cellular mechanisms. The preparation of nano vaccine: 3s-PLGA-PO-PEG/HA nanoparticles loaded OVA (PHO) were formulated by a double emulsion ($W_1/O/W_2$) solvent evaporation method and modified with HA. The PHO was taken up by APCs following recognition by CD44 receptor on APCs. The nanoparticles would be splitting in H_2O_2 environment in cells. The exogenous NPs loaded antigen were processed by endo/lysosomes following presented to $CD4^+$ T cells via MHC II pathway. The NPs also could escape lysosome phagocytosis and would be dissembled in H_2O_2 environment. The antigen would be presented to $CD8^+$ T cells via MHC I pathway.

Acknowledgment

The authors thank for the National Natural Science Funds of China (31771097, 31770968, 31600743), Tianjin Research Program of Application Foundation and Advanced Technology (17JCZDJC37400, 17JCZDJC33400, 16JCQNJC13900), Science and Technology Support Program of Tianjin (14RCGFSY00146). CAMS Innovation Fund for Medical Sciences (CIFMS 2017-I2M-1-016), European Research Council FP7 StG grant243261, and British Council Global Innovation Initiative grant.

Reference

1. Yoo, J. W.; Irvine, D. J.; Discher, D. E.; Mitragotri, S. Bio-inspired, bioengineered and biomimetic drug delivery carriers. *Nat Rev Drug Discov* **2011**,*10*, (7), 521-35.
2. Harisinghani, M. G.; Barentsz, J.; Hahn, P. F.; Deserno, W. M.; Tabatabaei, S.; van de Kaa, C. H.; de la Rosette, J.; Weissleder, R. Noninvasive detection of clinically occult lymph-node metastases in prostate cancer. *N Engl J Med* **2003**,*348*, (25), 2491-9.
3. Zamboni, W. C.; Torchilin, V.; Patri, A. K.; Hrkach, J.; Stern, S.; Lee, R.; Nel, A.; Panaro, N. J.; Grodzinski, P. Best practices in cancer nanotechnology: perspective from NCI nanotechnology alliance. *Clin Cancer Res* **2012**,*18*, (12), 3229-41.
4. Dobrovolskaia, M. A.; McNeil, S. E. Immunological properties of engineered nanomaterials. *Nat Nanotechnol* **2007**,*2*, (8), 469-78.
5. Fonseca, S. B.; Pereira, M. P.; Kelley, S. O. Recent advances in the use of cell-penetrating peptides for medical and biological applications. *Adv Drug Deliv Rev* **2009**,*61*, (11), 953-64.
6. Lallana, E.; Rios de la Rosa, J. M.; Tirella, A.; Pelliccia, M.; Gennari, A.; Stratford, I. J.; Puri, S.; Ashford, M.; Tirelli, N. Chitosan/Hyaluronic Acid Nanoparticles: Rational Design Revisited for RNA Delivery. *Mol Pharm* **2017**,*14*, (7), 2422-2436.
7. Kikuchi, S.; Griffin, C. T.; Wang, S. S.; Bissell, D. M. Role of CD44 in epithelial wound repair: migration of rat hepatic stellate cells utilizes hyaluronic acid and CD44v6. *J Biol Chem* **2005**,*280*, (15), 15398-404.
8. Jiang, D.; Liang, J.; Noble, P. W. Hyaluronan as an immune regulator in human diseases. *Physiol Rev* **2011**,*91*, (1), 221-64.
9. Jensen, P. V.; Larsson, L. I. Actin microdomains on endothelial cells: association with CD44, ERM proteins, and signaling molecules during quiescence and wound healing. *Histochem Cell Biol* **2004**,*121*, (5), 361-9.
10. Chen, J.; Ouyang, J.; Chen, Q.; Deng, C.; Meng, F.; Zhang, J.; Cheng, R.; Lan, Q.; Zhong, Z. EGFR and CD44 Dual-Targeted Multifunctional Hyaluronic Acid Nanogels Boost Protein Delivery to Ovarian

- and Breast Cancers In Vitro and In Vivo. *ACS Appl Mater Interfaces* **2017**,*9*, (28), 24140-24147.
11. Yun, Y. H.; Goetz, D. J.; Yellen, P.; Chen, W. Hyaluronan microspheres for sustained gene delivery and site-specific targeting. *Biomaterials* **2004**,*25*, (1), 147-57.
 12. Choi, K. Y.; Yoon, H. Y.; Kim, J. H.; Bae, S. M.; Park, R. W.; Kang, Y. M.; Kim, I. S.; Kwon, I. C.; Choi, K.; Jeong, S. Y.; Kim, K.; Park, J. H. Smart nanocarrier based on PEGylated hyaluronic acid for cancer therapy. *ACS Nano* **2011**,*5*, (11), 8591-9.
 13. Bae, S.; Park, M.; Kang, C.; Dilmen, S.; Kang, T. H.; Kang, D. G.; Ke, Q.; Lee, S. U.; Lee, D.; Kang, P. M. Hydrogen Peroxide-Responsive Nanoparticle Reduces Myocardial Ischemia/Reperfusion Injury. *J Am Heart Assoc* **2016**,*5*, (11).
 14. Zhu, X.; Liu, C.; Duan, J.; Liang, X.; Li, X.; Sun, H.; Kong, D.; Yang, J. Synthesis of three-arm block copolymer poly(lactic-co-glycolic acid)-poly(ethylene glycol) with oxalyl chloride and its application in hydrophobic drug delivery. *Int J Nanomedicine* **2016**,*11*, 6065-6077.
 15. Zhu, X.; Xie, H.; Liang, X.; Li, X.; Duan, J.; Chen, Y.; Yang, Z.; Liu, C.; Wang, C.; Zhang, H.; Fang, Q.; Sun, H.; Li, C.; Li, Y.; Wang, C.; Song, C.; Zeng, Y.; Yang, J. Bilayered Nanoparticles with Sequential Release of VEGF Gene and Paclitaxel for Restenosis Inhibition in Atherosclerosis. *ACS Appl Mater Interfaces* **2017**,*9*, (33), 27522-27532.
 16. Ma, Y.; Zhuang, Y.; Xie, X.; Wang, C.; Wang, F.; Zhou, D.; Zeng, J.; Cai, L. The role of surface charge density in cationic liposome-promoted dendritic cell maturation and vaccine-induced immune responses. *Nanoscale* **2011**,*3*, (5), 2307-14.
 17. Mesa, C.; de Leon, J.; Fernandez, L. E. Very small size proteoliposomes derived from *Neisseria meningitidis*: An effective adjuvant for generation of CTL responses to peptide and protein antigens. *Vaccine* **2006**,*24*, (14), 2692-9.
 18. Zhang, C.; Shi, G.; Zhang, J.; Song, H.; Niu, J.; Shi, S.; Huang, P.; Wang, Y.; Wang, W.; Li, C.; Kong, D. Targeted antigen delivery to dendritic cell via functionalized alginate nanoparticles for cancer immunotherapy. *J Control Release* **2017**,*256*, 170-181.
 19. Panagioti, E.; Redeker, A.; van Duikeren, S.; Franken, K. L.; Drijfhout, J. W.; van der Burg, S. H.; Arens, R. The Breadth of Synthetic Long Peptide Vaccine-Induced CD8+ T Cell Responses Determines the Efficacy against Mouse Cytomegalovirus Infection. *PLoS Pathog* **2016**,*12*, (9), e1005895.
 20. Dzieciuch-Rojek, M.; Poojari, C.; Bednar, J.; Bunker, A.; Kozik, B.; Nowakowska, M.; Vattulainen, I.; Wydro, P.; Kepczynski, M.; Rog, T. Effects of Membrane PEGylation on Entry and Location of Antifungal Drug Itraconazole and Their Pharmacological Implications. *Mol Pharm* **2017**,*14*, (4), 1057-1070.
 21. Manolova, V.; Flace, A.; Bauer, M.; Schwarz, K.; Saudan, P.; Bachmann, M. F. Nanoparticles target distinct dendritic cell populations according to their size. *Eur J Immunol* **2008**,*38*, (5), 1404-13.
 22. Kim, S.; Park, H.; Song, Y.; Hong, D.; Kim, O.; Jo, E.; Khang, G.; Lee, D. Reduction of oxidative stress by p-hydroxybenzyl alcohol-containing biodegradable polyoxalate nanoparticulate antioxidant. *Biomaterials* **2011**,*32*, (11), 3021-9.
 23. Yang, Y. W.; Hsu, P. Y. The effect of poly(D,L-lactide-co-glycolide) microparticles with polyelectrolyte self-assembled multilayer surfaces on the cross-presentation of exogenous antigens. *Biomaterials* **2008**,*29*, (16), 2516-26.
 24. Zhang, C.; Zhang, J.; Shi, G.; Song, H.; Shi, S.; Zhang, X.; Huang, P.; Wang, Z.; Wang, W.; Wang, C.; Kong, D.; Li, C. A Light Responsive Nanoparticle-Based Delivery System Using Pheophorbide A Graft Polyethylenimine for Dendritic Cell-Based Cancer Immunotherapy. *Mol Pharm* **2017**,*14*, (5), 1760-1770.
 25. Singh, D.; Somani, V. K.; Aggarwal, S.; Bhatnagar, R. PLGA (85:15) nanoparticle based delivery of rL7/L12 ribosomal protein in mice protects against *Brucella abortus* 544 infection: A promising alternate

to traditional adjuvants. *Mol Immunol* **2015**,*68*, (2 Pt A), 272-9.

26. Jiang, H.; Wang, Q.; Sun, X. Lymph node targeting strategies to improve vaccination efficacy. *J Control Release* **2017**.

27. Wang, C.; Zhuang, Y.; Zhang, Y.; Luo, Z.; Gao, N.; Li, P.; Pan, H.; Cai, L.; Ma, Y. Toll-like receptor 3 agonist complexed with cationic liposome augments vaccine-elicited antitumor immunity by enhancing TLR3-IRF3 signaling and type I interferons in dendritic cells. *Vaccine* **2012**,*30*, (32), 4790-9.

28. Heath, W. R.; Carbone, F. R. Cross-presentation in viral immunity and self-tolerance. *Nat Rev Immunol* **2001**,*1*, (2), 126-34.

29. Mueller, S. N.; Tian, S.; DeSimone, J. M. Rapid and Persistent Delivery of Antigen by Lymph Node Targeting PRINT Nanoparticle Vaccine Carrier To Promote Humoral Immunity. *Mol Pharm* **2015**,*12*, (5), 1356-65.

30. Purkerson, J.; Isakson, P. A two-signal model for regulation of immunoglobulin isotype switching. *FASEB J* **1992**,*6*, (14), 3245-52.

31. Kipnis, A.; Irwin, S.; Izzo, A. A.; Basaraba, R. J.; Orme, I. M. Memory T lymphocytes generated by Mycobacterium bovis BCG vaccination reside within a CD4⁺ CD44^{lo} CD62⁺ ligand^(hi) population. *Infect Immun* **2005**,*73*, (11), 7759-64.

32. Liu, L.; Ma, P.; Wang, H.; Zhang, C.; Sun, H.; Wang, C.; Song, C.; Leng, X.; Kong, D.; Ma, G. Immune responses to vaccines delivered by encapsulation into and/or adsorption onto cationic lipid-PLGA hybrid nanoparticles. *J Control Release* **2016**,*225*, 230-9.